ADVANCED NONLINEAR MODELLING TECHNIQUES FOR SWITCHED RELUCTANCE MACHINES

Frederik D'hulster ; Kurt Stockman ; Jan Desmet
Hogeschool West-Vlaanderen dept. PIH
Graaf Karel de Goedelaan 5
B-8500 KORTRIJK (Belgium)
frederik.dhulster@howest.be

Ronnie Belmans
Katholieke Universiteit Leuven dept. ESAT
Kasteelpark Arenberg 10
B-3001 LEUVEN (Belgium)
ronnie.belmans@esat.kuleuven.ac.be

Abstract

This paper gives an overview of different modelling techniques to describe the nonlinear behaviour of both saturated switched reluctance machine (SRM) and power electronic converter. The current research contributes by comparing the de-coupled single-phase superposition method (lookup-tables) with a coupled analysis between drive model in Matlab/Simulink® and finite element model of the SRM motor. Experimental characterization techniques as well as finite element techniques are used to obtain the single-phase flux-linkage data. Transient electromagnetic analysis using the finite element method, coupled with a drive model and optimization strategy in Matlab/Simulink®, results in a more accurate SRM modelling. These results are more accurate because the mutual coupling between different phases is taken into account. Using this direct coupling, a complete analysis of the motor behaviour (local saturation, iron losses, …) can be modelled with the finite element software, keeping the complex drive and control strategy in Matlab/Simulink®. At every time step of the discrete solver, data is exchanged between the drive model and the coupled electric circuit of the finite element analysis.
Simulation results are compared with measurements of flux-linkage, torque, phase current and iron losses. Pro's and contra's of the coupled and de-coupled modelling technique are discussed.

Key Words
switched reluctance machine, advanced modelling, finite elements, drive optimization

1. Introduction

Designers of electromechanical devices are facing ever-increasing demands to model complete and sometimes complex systems, including the electromagnetic device, power electronic converter (supply, inverter,…), control system and the kinematics of the mechanical load.

Switched reluctance machines are relatively simple electric machines but are difficult to model and control. Due to their control-complexity, SRM-drives are only integrated in a few market-segments. Because of some particular advantages, SRM-drives could be implemented in applications where features as robustness, wide speed range, efficiency or high dynamics are required. Different papers have been published [1-9], dealing with different aspects of SRM-modelling. SRM-drive optimization for different customer demands (maximum efficiency, maximum torque, minimum noise and vibration, …) results in need for an automated identification and optimization platform. This platform must be based on an accurate nonlinear model. Using the model, rules can be deducted between different drive parameters and the input functions of the optimization platform. The nonlinear SRM-behaviour can be incorporated into the drive model using offline single phase characterization data or through a direct coupling between the drive model in Matlab/Simulink® and a finite element analysis of the motor geometry. This coupling results in more accurate flux-linkage estimation, taking into account the mutual coupling of all phases. Both techniques are analyzed and discussed in this paper.

2. Basic principles of SRM's

The concept of a switched reluctance machine is very simple. It consists of stator and rotor poles, made of laminated steel with high magnetic permeability. Only the stator poles are excited by coils. A typical configuration is shown in Figure 1, with 8 stator en 6 rotor poles, a so-called '8/6 SRM'. With 8 coils on the stator, 4 phases are created with the corresponding coils in parallel. Two extreme rotor positions are defined: unaligned (-30°) and aligned (0°), as can be seen in the flux distribution plots of Figure 1. A sequence of anti-clockwise excitations of different phases results in a clockwise rotation of the rotor due to a positive torque generation. SRM's are characterized by a flux-linkage ψ and inductance L, varying with position and current. The position-dependent behaviour is due to the geometry of the overlapping stator and rotor teeth.

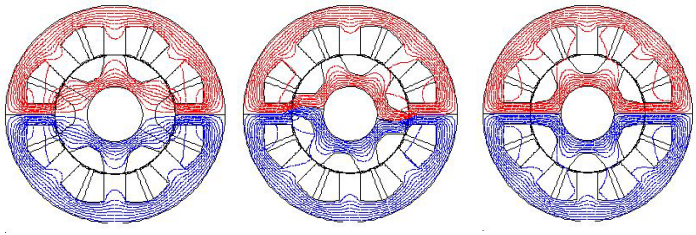

Unaligned (-30°) *Positive torque (-10°)* *Aligned (0°)*

Figure 1. Flux-distribution at different SRM rotor-positions for a single phase excitation

In most SRM-applications, saturation occurs, resulting in a nonlinear inductance and flux-linkage. This nonlinear behaviour explains the difficulty in modelling and controlling SRM-drives. Figure 3 shows a typical flux-linkage ψ versus current i graph of a single phase for different rotor positions θ. This graph fully characterizes the electromagnetic behaviour of the SRM. In the aligned position, flux density is much higher due to low magnetic reluctance, resulting in saturation, even at low current levels. In the unaligned position, the magnetic reluctance is so high that saturation never can be achieved. This characterization of a single phase can be obtained by measurements or finite element modelling (FEM).

3. Electromagnetic system equations

In a 8/6 SRM configuration, there are always one or two phases excited. During a phase-excitation, the DC-link voltage u is applied and the resulting current depends on the resistance R and the time-derivation of the flux-linkage ψ. Figure 2 represents the electrical equivalent of a stator phase. All derived formulas are valid for one excited stator phase. The voltage-equation of a stator phase can be written, using partial derivatives (ω_m = angular rotor speed):

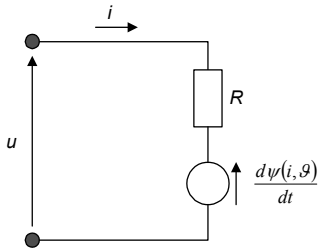

Figure 2: Electrical equivalent of a stator phase

$$u = R.i + \frac{\partial \psi(i,\theta)}{\partial i}.\frac{di}{dt} + \frac{\partial \psi(i,\theta)}{\partial \theta}.\omega_m \qquad (1)$$

The electromagnetic system equation (1) can be rewritten to:

$$\frac{di}{dt} = \frac{1}{\frac{\partial \psi(i,\theta)}{\partial i}}.\left[u - R.i - \frac{\partial \psi(i,\theta)}{\partial \theta}.\omega_m\right] \qquad (2)$$

For a given SRM characterization (flux-linkage $\psi(i,\theta)$), the phase current i can be calculated from equation (2). In order to derive an expression for the electromagnetic torque of a SRM, an energy-balance must be written. The electrical energy is used for electromagnetic torque production or is stored into the magnetic field. Magnetic co-energy is used to derive a general formula for the electromagnetic torque production:

$$T_m(i,\theta) = \left.\frac{\partial W_{co}(i,\theta)}{\partial \theta}\right|_{i=cst} = \int_0^i \frac{\partial \psi(i,\theta)}{\partial \theta}.di \qquad (3)$$

Equation (3) gives an expression for instantaneous torque in terms of the differential change in co-energy with respect to position, evaluated at a constant phase current.

Graphically, the mechanical energy W_m is the surface, enclosed in the energy-conversion graph, by exciting a phase. Figure 3 shows an example (ω_{m1} = 100 rad/s, ω_{m2} = 250 rad/s, i_{ref} = 10 A, u = 310 V). Due to the high back-emf at rotor speed ω_{m2}, the reference current cannot be sustained. The average torque is equal to the area enclosed by the change in co-energy divided by the change in position. The instantaneous torque is the differential co-energy as the change in position tends toward zero. According to equation (3), each phase produces a torque. The global electromagnetic torque generation T_{SR} of a SRM can be approximated by (superposition method):

$$T_{SR}(i,\theta) = \sum_{k=1}^{n_S} T_{mk}(i,\theta) \qquad (4)$$

with: n_S = number of excited stator phases

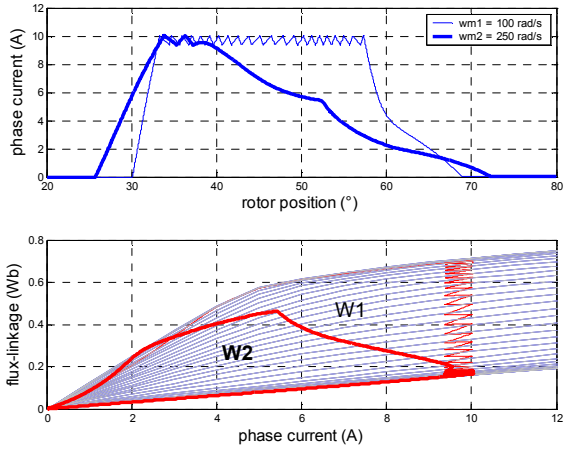

Figure 3. Phase current and energy conversion during single-phase excitation (ω_{m1} = 100 rad/s, ω_{m2} = 250 rad/s, i_{ref} = 10 A, u = 290 V, optimal a_{ON} and a_{OFF} for maximum torque)

Using equation (4) as an expression for the electromagnetic torque production, a three-dimensional graph, representing the electromagnetic torque for one phase, can be built (Figure 4). Two calculation methods can be used to construct this torque-graph:

- partial derivative (to θ) of the co-energy
- integral over current-range of the partial derivative (to θ) of the flux-linkage (further called $p_\theta(i,\theta)$)

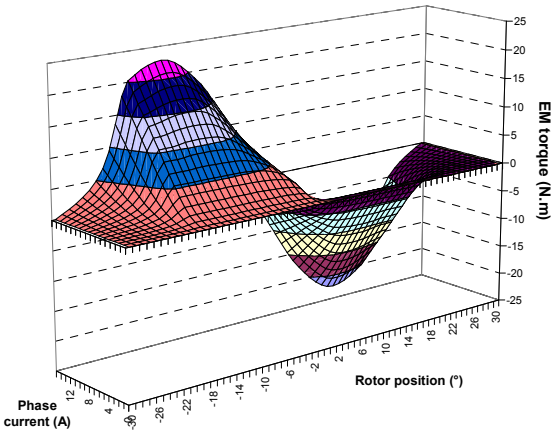

Figure 4. Single phase torque behaviour of a SRM (Flux2D®)

This graph fully describes the torque behaviour of a SRM in function of phase current and rotor position. Figure 4 clearly shows that most of the torque generation is concentrated in a narrow interval between unaligned and aligned position. Equation (2) and (3) are the fundamental equations to represent the behaviour of phase current and electromagnetic torque during the rotation of a SRM. These equations depend on both current and position dependant parameters, namely:

$$p_i(i,\theta)=\frac{\partial\psi(i,\theta)}{\partial i} \quad ; \quad p_\theta(i,\theta)=\frac{\partial\psi(i,\theta)}{\partial\theta} \qquad (5)$$

Instead of characterizing a SRM by means of its flux-linkage graph $\psi(i,\theta)$, another approach consists of the partial derivatives $p_i\,(i,\theta)$ and $p_\theta\,(i,\theta)$. Parameter $p_i\,(i,\theta)$ represents the phase inductance (Figure 5) and $p_\theta(i,\theta)$ the back-emf coefficient (Figure 6). The inductance $p_i\,(i,\theta)$ remains nearly constant when phase current is high, due to the high saturation in the overlapping poles. For low phase current levels, no saturation occurs and a linear relation between inductance and rotor position exists during pole overlapping.

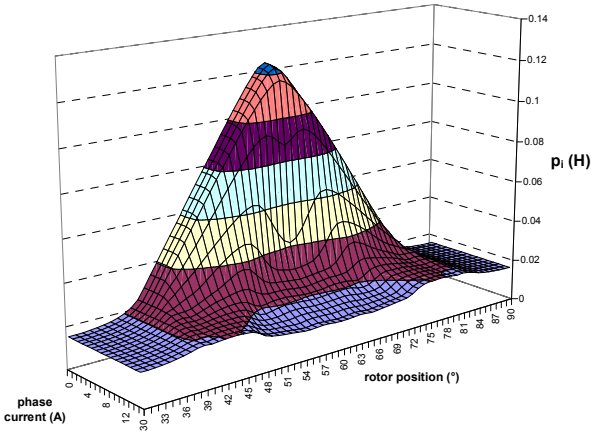

Figure 5. Flux-linkage partial derivative to i (p_i) (inductance)

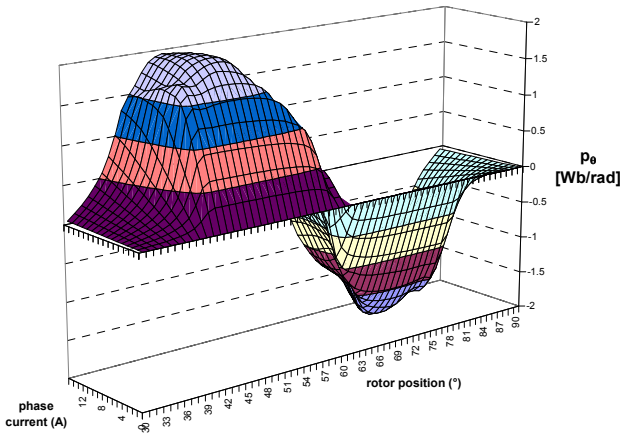

Figure 6. Flux-linkage partial derivative to θ (p_θ) (back-emf coefficient)

Using these partial derivatives, different control angle strategies could be analyzed and finally optimized. E.g. the start of the inductance raising can be used to calculate an efficient turn-on angle a_{ON} to activate the phase. Before this pole overlapping, the torque generation is minimal compared to the Joule-losses in the phase winding. Another optimization could be performed for maximum mean torque production using the area in the energy-conversion diagram.

4. SRM single-phase characterization

The flux-linkage partial derivatives (5) fully describe the SRM electromagnetic behaviour. This data can be achieved using finite element modelling with measured material magnetization (BH) data or by flux-linkage measurement on an experimental test setup.

4.1 Finite element analysis

A multiparametric (i,θ) model is built and solved through magnetostatic computation with two-dimensional triangular elements. The uniform mesh pattern is created using mesh density on points. Due to symmetry, only half a 8/6 motor is to be represented. Figure 7 shows a part of the meshed SRM. A rotating airgap (0.38 mm) connects the stator with the moving rotor. Figure 1 shows the equiflux-lines at different rotor positions. Because of the length of the rotor, which is 3 times the rotor diameter, a two-dimensional model is used. For shorter SRM's, the end-effects can be modelled by an inductance in the electric circuit or a three-dimensional model must be built. Using

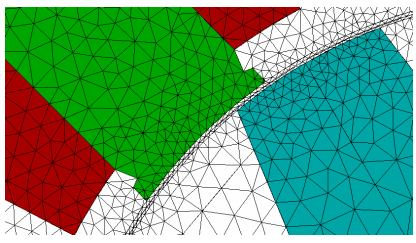

Figure 7. Two-dimensional FE-model (Flux2D®)

a stacking factor of 0.93, the effective stack iron length is taken into account. The magnetization (BH)-data of the stack material is measured on a standard Epstein frame and is stored in the materials database of the FE-analysis.

4.2 Experimental test setup

Different papers are published in which automated SRM-characterization systems are presented ([10], [11]). A test setup is built using a PMSM load machine and torque transducer (Figure 8). The load machine operates in speed-control mode and the SRM in current-control mode. A braking resistor at the load machine (generating) dissipates the energy from the SRM (motoring). This setup enables the measurement of static torque, flux-linkage and torque-speed characteristics.

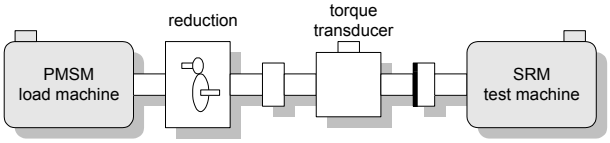

Figure 8. Experimental test setup

Miller [12] describes a direct method to measure the magnetization curves (ψ-i-θ) using the voltage equation:

$$u = R.i + \frac{d\psi(i,\theta)}{dt} \qquad (6)$$

Flux-linkage is calculated by integrating the source voltage minus the resistive voltage drop. To obtain proper results, the resistance R must be chosen carefully to obtain zero flux at zero current (Figure 9). Automation is achieved through a position controlled load machine, which gradually moves the rotor of the SRM. Low voltage excitation is used to minimize the effect of induced currents in coupled conducting paths. The test setup is equipped with a DS1104 dSpace®-controller board.

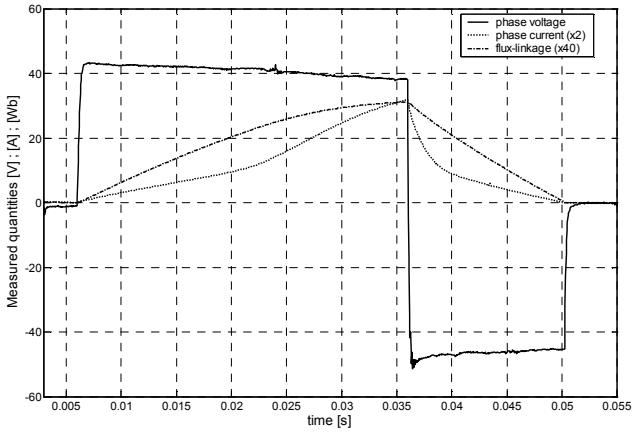

Figure 9. Single phase flux-linkage characterization (aligned position) (measurement)

Figure 10 compares the calculated single-phase static torque with the measurements on the test setup.

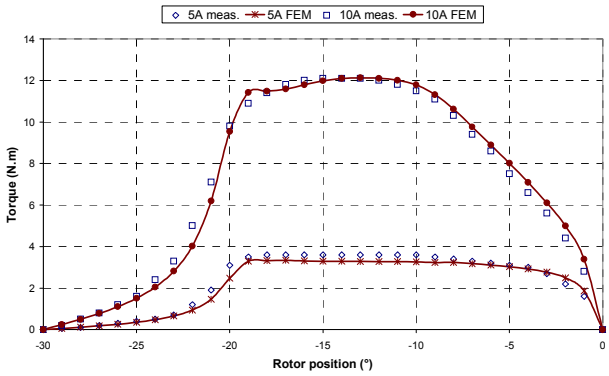

Figure 10. Single-phase torque generation (simulation vs. measurement)

5. SRM drive modelling techniques

A model of the complete SRM with drive consists of the motor-model (electromagnetic system equation (2) and (4)), a phase-activation control strategy, a current hysteresis controller, a speed controller and a load-model. The current hysteresis controller uses soft-chopping (ON, FREEWHEEL and OFF-state) to maintain the reference current. In all simulation results, these angles are optimized to obtain maximum mean torque for every speed and reference current. A first technique uses the single-phase flux-linkage characterization data, obtained from measurements or FE-analysis. For multiple phase excitations, a superposition of the torque generation of each single phase is used. A second and more accurate modelling technique calculates the torque-generation at every time-step using a direct coupling between a model of the SRM-drive and a FE-analysis of the SRM-geometry.

5.1 Superposition of single-phase characterization data

The SRM with drive is modelled in Matlab/Simulink® using the superposition method, yielding a complete four-quadrant control. The single-phase flux-linkage partial derivatives are stored in lookup tables. The global electromagnetic torque is calculated using a superposition of the single-phase torque characteristics, according to (4). All phase currents are calculated using the electromagnetic system equation (2). The simulation results, containing the current in all phases, the instantaneous motor torque and the rotor speed, are summarized in Figure 11 for two quadrants of the motor.

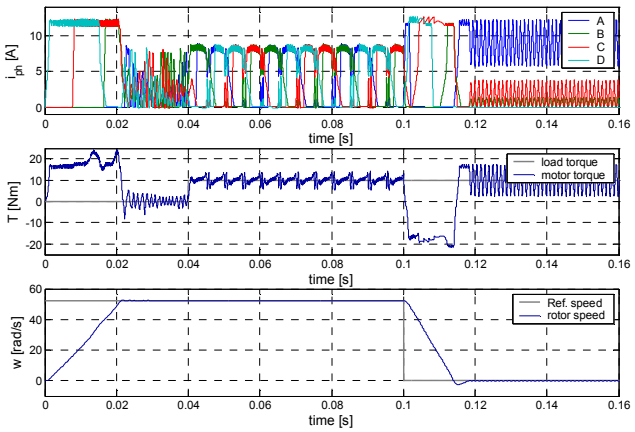

Figure 11. SRM control using superposition of single-phase characterization data (Matlab/Simulink®)

5.2 Direct coupling with FE-analysis

Previous modelling technique uses single-phase flux-linkage data to calculate the torque, generated by simultaneously excited phases, by superposing the shifted torque characteristics. In this way, the computationally intensive electromagnetic finite element analysis is de-coupled from the time-stepping simulation. In reality, due to adjacent excitations, different polarization of the stator occurs, resulting in different flux-paths. Figure 12 illustrates some flux-patterns during simultaneous phase excitations. This results in a higher reluctance for excitation combination AD, compared with AB, BC and CD.

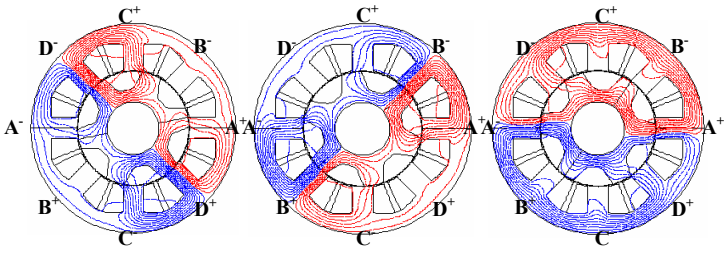

Figure 12. Simultaneous phase excitations

The coupling between drive model and FE-analysis is represented in Figure 13. The input parameters for the FE-analysis are the applied phase-voltages and the rotor speed. The output parameters are the phase-currents and the instantaneous electromagnetic torque. At every time-step (t_s = 50 µs), data is exchanged between the drive model and the FE-analysis. The coupled electric circuit model consists of phase coils with a programmable voltage source and a switch to obtain a unidirectional current. A transient magnetic analysis is used, in which a time-stepping process is employed.

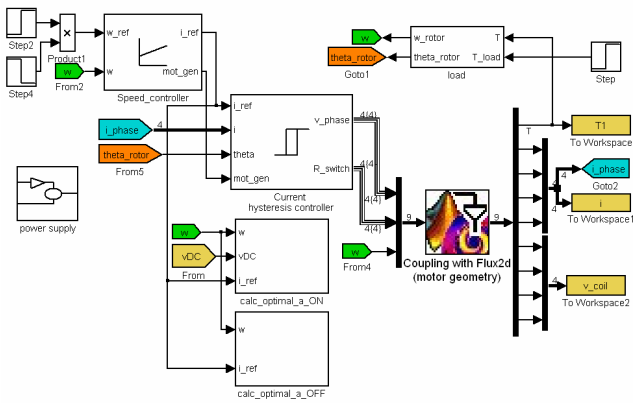

Figure 13. Direct coupling between drive model and FE-analysis of motor geometry

This technique allows us to split the drive and load model in Matlab/Simulink® from the motor model in Flux2D®. This method has the great advantage that a complex drive model can be used in combination with accurate flux-linkage calculation, taking into account the mutual coupling between adjacent phases and induced voltages in inactive phases. The disadvantage is the higher calculation time.

5.3Validation of both modelling techniques

The model validation is performed through current- and torque-measurements on the test setup. Figure 14 compares the measured and simulated soft-chopping of the current hysteresis controller at low and high rotor speed. The sample time of the current capture (dSpace® DS1104) is 40µs, limiting the full representation of the chopping.

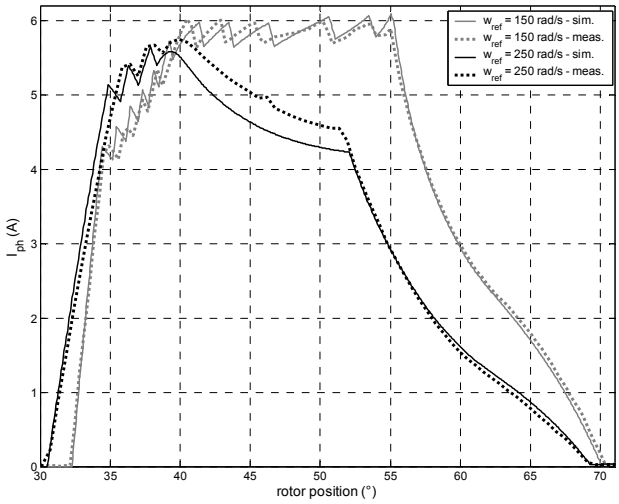

Figure 14. Validation of current hysteresis controller (i_{ref} = 6A) (simulation with superposition method vs. measurements)

With the topology of a four phase SRM, a choice between two (A-C and B-D) or four (one for each phase) current transducers can be made. The number of current

transducers has a significant influence on the torque performance of the SRM drive. Figure 14 clearly shows that chopping already starts before the reference phase current is achieved, due to a remaining current in the alternating phase. This loss of surface in the energy-conversion plane results in a loss of mean torque production.
Figure 15 compares the instantaneous torque calculation of both modelling techniques with the measurements. The torque-dip for AD excitation is clearly visible in the FE-coupling and the measurements but does not appear in the single-phase superposition method. This torque dip is caused by the increased reluctance due to equal polarization of phases A and D (Figure 12).

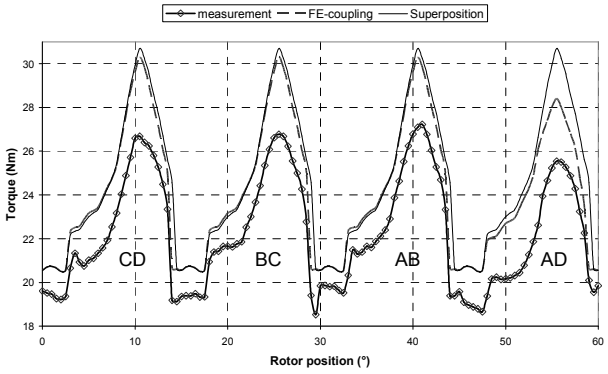

Figure 15. Torque during simultaneous excited phases
(i_{ref} = 14A ; ω_m = 50 rad/s ; u = 290 V ; a_{ON} = 32.9° ; a_{OFF} = 58.8°)

Figure 15 shows that the simulated torque is always larger then the measurements, due to the iron losses in the SRM stack material. To obtain a more accurate SRM model, the iron losses must be estimated.

5.4 Case study: estimation of iron losses in SRM's

The losses in a switched reluctance motor mainly consist of iron and copper losses. The prediction of copper losses is relatively simple when the current waveform is known. Estimation of iron losses is much more complicated. The iron losses are function of the amplitude and frequency of the induction (B) waveform in the stack material. Figure 16 illustrates the iron losses of stack material during sinusoidal excitation, measured on a standard Epstein frame. They can be expressed by:

$$\log(P) = C_1 + C_2 \cdot \log(f) \qquad (7)$$

However, inside the stator and rotor of a SRM, the flux and induction distribution is not sinusoidal at all. [14] describes a method to estimate the iron losses of a SRM,using a superposition of harmonic components of the induction waveforms. Using a simplified graphical technique to obtain the periodic induction waveforms in different motor parts (rotor core, rotor pole, stator core, stator pole), Fourier analysis is applied to extract the ac components. Superposition of the iron losses of each frequency component, according to Figure 16, results in an estimation of the total iron losses. This approach is justified within small deviations from the operating point since the nonlinear B-H characteristics can be approximated by an infinite number of piecewise linear characteristics.

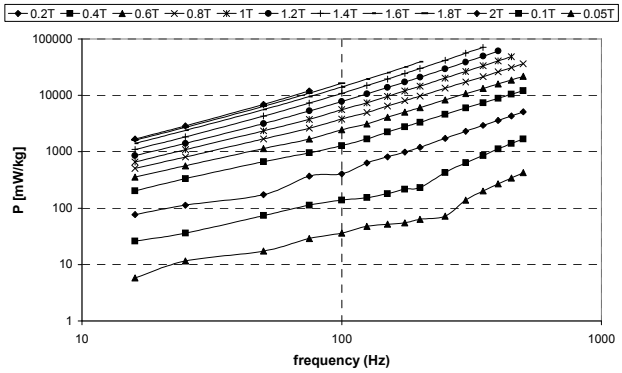

Figure 16. Iron losses of stack material during sinusoïdal excitation (measurement)

Previous simplified graphical method to define the induction waveforms is not that flexible and accurate. Many parameters in the control strategy (turn-on angle, turn-off angle, freewheel angle, …) influence the induction waveform in the core and poles of stator and rotor. When applying the direct coupling between SRM-drive and FE-model of the motor geometry, the induction waveforms can be calculated for every operating point. This is realized by integrating a single-turn coil in the stator pole, stator core, rotor pole and rotor core (Figure 17). The induced coil voltage e_{coil} is returned to Matlab/Simulink® for the calculation of the induction B, using equation:

$$B = \frac{1}{A}\int e_{coil}\,.dt \qquad (8)$$

with: A = surface, enclosed by coil

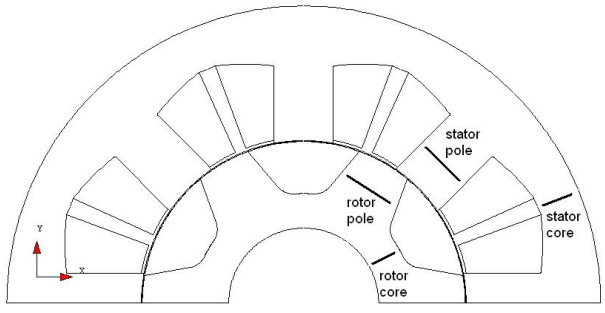

Figure 17. Single turn coils in FEM to calculate iron losses

This direct coupling has the great advantage that induction waveforms in every point of the motor geometry can be analysed, even with a complex SRM drive control strategy.

Figure 18 shows the coupled electric circuit for the calculation of phase currents and induced voltages in the single turn coils. The induction waveforms in the different regions are represented in Figure 19. The harmonic analysis of the induction waveform in the stator pole is shown in Figure 20. Superposition of the losses of each harmonic component results in an estimation of the global iron losses.

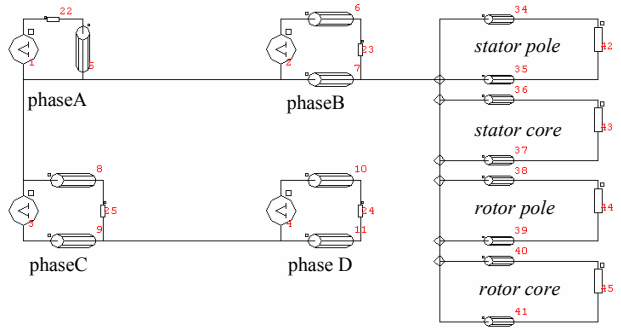

Figure 18. Coupled electric circuit in FEM, extended for calculation of iron losses

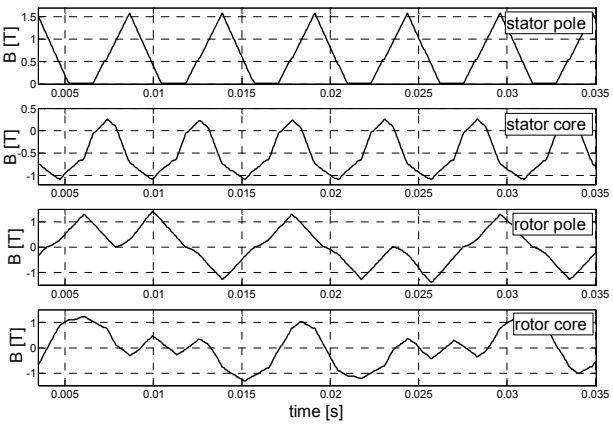

Figure 19. Induction waveforms in stator and rotor parts of the SRM (i_{ref} = 10 A ; ω_{ref} = 200 rad/s)

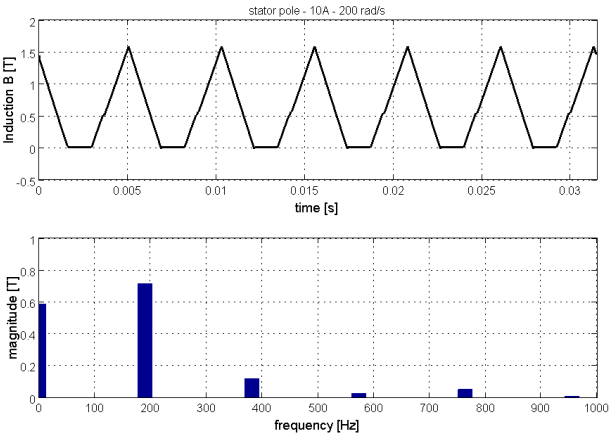

Figure 20. Time- and frequency analysis of induction in stator pole (i_{ref} = 10 A ; ω_{ref} = 200 rad/s)

To validate the estimation of iron losses, measurements of electrical, mechanical and Joule energy must be performed on the test setup. Iron losses can be calculated using (9):

$$P_{Fe} = P_{el} - P_{mech} - P_{Joule} \tag{9}$$

When analysing eq. (9), the iron losses are very small compared to the electrical and mechanical energy. This error propagation can result in a global error on the iron losses measurement of up to 20%. For this reason, accurate measurement of SRM iron losses is very difficult. Figure 21 compares the simulation results, using the direct coupling with FE-analysis, with the measurements on the test setup. The difference between simulation and measurement is beneath 15%, in this way approving the simulation tool.

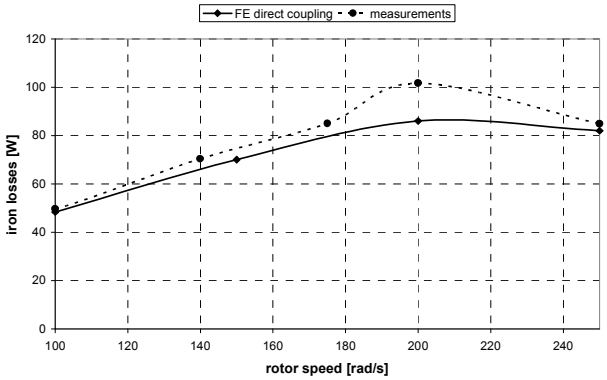

Figure 21. Estimation of iron losses (i_{ref} = 5 A) (simulation vs. measurements)

With this iron losses information, the torque-speed behaviour of the SRM is modelled and compared with measurements (Figure 22). Including an estimation of the iron losses results in better torque-speed prediction.

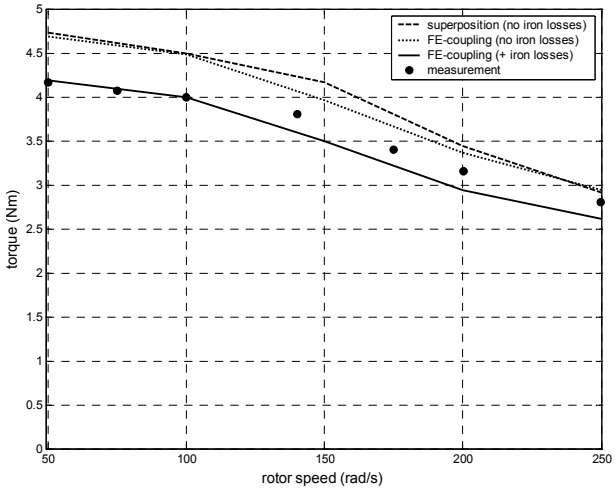

Figure 22. Torque-speed behaviour (i_{ref} = 5 A) (simulation versus measurements)

6. Conclusion

Different nonlinear modelling techniques for SRM's are discussed in this paper. A first method uses the characterization data (measured or obtained by FEM) of a single phase and superposes the torque characteristics to model simultaneous phase-excitations. A second method uses a coupling between the drive model and a FE-analysis to calculate the torque behaviour of simultaneously excited adjacent phases. Those results are more accurate because the mutual inductance is taken into account. Finally, this coupling is applied as a simulation tool for the estimation of iron losses in SRM's. Control of SRM's can be defined through different strategies, which optimize one single parameter of the drive concept. A flexible optimization platform generates optimized drive parameters through an input function (application demands) and a set of rules (relations between drive parameters and input function). Those rules are generated using the nonlinear model. The accuracy of the optimization procedure strongly depends on the model accuracy.

7. Appendix

The tested SRM has following characteristics:
4-phase 8/6 – P_{rated} = 700 W – T_{peak} = 22 Nm (15 A)

8. Acknowledgement

The authors wish to thank the Flemish Government (IWT) for granting the research project "Bepaling van de optimale stuur- en regelparameters voor systemen met SR-motor aandrijving. Ontwerp van een ontwikkelingsplatform."

References

[1] Nicolas J. Nagel, Robert D. Lorenz, Modelling of a switched reluctance motor using an operating point analysis and the unsaturated torque equation, *IEEE Trans. on Industry Applications*, *vol. 36*, May/June 2000, pp. 714-722.

[2] Wei Min Chan, W. F. Weldon, Development of a simple nonlinear switched reluctance motor model using measured flux linkage data and curve fit, in *Conf. Rec. IEEE-IAS Annual Meeting*, New Orleans, LA, Oct. 5-9, 1997, pp 318-325.

[3] V. Hrabovcova, P. Rafajdus, M. Licko, L. Janousek, Modelling of the dynamic operation of the switched reluctance motor drive by Simulink, in *Conf. Proc. SPEEDAM*, Sorrento (It.), June 3-5, 1998, pp. 61-66.

[4] Vladan Vuji, Slobodan N. Vukosavic, A simple nonlinear model of the switched reluctance motor, *IEEE Trans. on Energy Conversion*, *vol. 15*, Dec. 2000, pp. 395-400.

[5] Christophe Roux, M.M. Morcos, A simple model for switched reluctance motors, *IEEE Power Engineering Review*, Oct. 2000, pp. 49-52.

[6] Sayeed Mir, Iqbal Husain, Malik E. Elbuluk, Switched reluctance motor modelling with on-line parameter identification, *IEEE Trans. on Industry Applications* , vol. 34, July/August 1998, pp. 776-783.

[7] C. Dragu, R. Belmans, Four-quadrant control of an 8/6 switched reluctance motor, in *Conf. Proc. ELECTROMOTION2001*, Bologna (It.), June 19-20, 2001, pp. 455-460.

[8] J. Mahdavi, G. Suresh, B. Fahimi, M. Ehsani, Dynamic modelling of non-linear SRM drive with Pspice, in *Conf. Rec. IEEE-IAS Annual Meeting*, New Orleans, LA, Oct. 5-9, 1997, pp 661-667.

[9] I.A. Viorel, G. Henneberger, Ilinca Tomescu, Ioana Vintiloiu, A new approach to the computation of the switched reluctance motor dynamic behaviour, in *Conf. Proc. ICEM2000*, Espoo (Fi.), August 28-30, 2000, pp. 1605-1608.

[10] Adrian David Cheok, Nesimi Ertugrul, Computer-based automated test-measurement system for determining magnetization characteristics of switched reluctance motors, *IEEE Trans. on Instrumentation and Measurement*, *vol. 50*, June 2001, pp. 690-696.

[11] V. Trifa, A. Graur, O. Rabulea, Labview virtual instrumentation for a switched reluctance motor, in *Proc. Ee2001*, Novi Sad (Yu.), Oct. 31 – Nov. 2, 2001, pp. 283-285.

[12] T.J.E. Miller, *Electronic control of switched reluctance machines (*Newnes Power Engineering Series, Oxford, 2001).

[13] T.J.E. Miller, *Switched reluctance motors and their control (*Oxford University Press and Magna Physics Publications (U.K), 1993).

[14] P. N. Materu, R. Krishnan, Estimation of switched reluctance motor losses, *IEEE Trans. on Industry Applications*, *vol. 28*, N° 3, May/June 1992, pp. 668-679.